A method for detection and characterization of structural non-linearities using the Hilbert transform and neural networks

V. Ondra[a,*], I.A. Sever[b], C.W. Schwingshackl[a]

[a] *Imperial College London, Mechanical Engineering, Exhibition Road, SW7 2AZ London, United Kingdom*
[b] *Rolls-Royce plc., DE24 8BJ Derby, United Kingdom*

Abstract

This paper presents a method for detection and characterization of structural non-linearities from a single frequency response function using the Hilbert transform in the frequency domain and artificial neural networks. A frequency response function is described based on its Hilbert transform using several common and newly introduced scalar parameters, termed non-linearity indexes, to create training data of the artificial neural network. This network is subsequently used to detect the existence of non-linearity and classify its type. The theoretical background of the method is given and its usage is demonstrated on different numerical test cases created by single degree of freedom non-linear systems and a lumped parameter multi degree of freedom system with a geometric non-linearity. The method is also applied to several experimentally measured frequency response functions obtained from a cantilever beam with a clearance non-linearity and an under-platform damper experimental rig with a complex friction contact interface. It is shown that the method is a fast and noise-robust means of detecting and characterizing non-linear behaviour from a single frequency response function.

Keywords: Non-linear system characterization, Hilbert transform, Neural network classification, Nonlinearity indexes

Highlights

- a tool for detection and characterization of structural non-linearities
- proposed non-linearity indexes describe FRFs based on the Hilbert transform
- the neural network is used to classify non-linear behaviour based on the non-linearity indexes
- successful characterization of several numerical and two experimental test cases is shown

Nomenclature

Symbol	Description
b	clearance size parameter [m]
c	linear damping coefficient [$\mathrm{N\,m^{-1}\,s^{-1}}$]
c_{nl}	non-linear (quadratic) damping coefficient [$\mathrm{N\,m^{-2}\,s^{-1}}$]
f	frequency [Hz]
f_0	undamped natural frequency [Hz]

*Corresponding author.
Email addresses: v.ondra14@imperial.ac.uk (V. Ondra), Ibrahim.Sever@Rolls-Royce.com (I.A. Sever), c.schwingshackl@imperial.ac.uk (C.W. Schwingshackl)

$f(x)$	activation (transfer) function
$F(t)$	excitation force [N]
F	amplitude of excitation force [N]
$\mathbf{F}(t)$	excitation force vector [N]
$g_{\mathrm{nl}}(x, \dot{x})$	non-linear restoring force [N]
$G(\omega)$	difference between an FRF and its Hilbert transform
$\mathbf{G}_{\mathrm{nl}}(\mathbf{x}, \dot{\mathbf{x}})$	non-linear restoring force matrix [N]
$H(\omega)$	frequency response function - receptance [$\mathrm{m\,N^{-1}}$]
$\mathrm{HTD}^{(n)}$	nth Hilbert transform describer
k	linear stiffness coefficient [$\mathrm{N\,m^{-1}}$]
k_{cl}	clearance stiffness coefficient [$\mathrm{N\,m^{-1}}$]
k_{nl}	cubic stiffness coefficient [$\mathrm{N\,m^{-3}}$]
$\mathbf{K}$	stiffness matrix [$\mathrm{N\,m^{-1}}$]
m	mass [kg]
$m(\omega)$	weight function
$M_H^{(n)}$	nth-order spectral moment
$\mathrm{n_h}$, $\mathrm{n_{sl}}$	number of harmonic components and spectral lines
$\mathbf{M}$	mass matrix [kg]
NLI_i	ith non-linearity index
$R_{H\tilde{H}}(\Delta\omega)$	cross-correlation
$\mathbf{S}$	scatter matrix
$\mathbf{U}$	matrix of principal component directions
w_{ij}^k	weight between ith and jth node of kth layer
x, $\dot{x}$, $\ddot{x}$	displacement [m], velocity [m s], acceleration [$\mathrm{m\,s^2}$]
$x_i^{(k)}$	signal at node i in layer k
$\mathbf{x}_s$	vector of samples
$\mathbf{x}$, $\dot{\mathbf{x}}$, $\ddot{\mathbf{x}}$	displacement [m], velocity [m s], acceleration [$\mathrm{m\,s^2}$] vectors
$\mathbf{X}_0$	displacement due to static forces [m]
$\mathbf{X}_j^c$, $\mathbf{X}_j^s$	cosine and sine harmonic coefficient [m]
$\mathbf{z}$	principal component scores
α, β	Rayleigh's proportional damping coefficients
γ_1	centre of gravity
γ_2, γ_3	moment of inertia about ω-axis and with respect to origin
Δf	frequency resolution [Hz]
$\Delta\omega$	angular frequency lag [$\mathrm{rad\,s^{-1}}$]
μN_{f}	Coulomb friction force [N]
σ	standard deviation
$\mathbf{\Sigma}$	diagonal matrix of relative contributions
$\varphi(\omega)$	phase [rad]
ω	angular frequency [$\mathrm{rad\,s^{-1}}$]
$\omega_{\min}$, $\omega_{\max}$	minimum and maximum angular frequency [$\mathrm{rad\,s^{-1}}$]
Ω	substitution of ω in integrand
$\bullet^*$	normalized attributes
$\tilde{\bullet}$	Hilbert transformed attributes
$\bar{\bullet}$	arithmetic mean
$\bullet^T$, $\bullet^{-1}$	matrix transpose and inverse
$\mathscr{H}\{\bullet\}$	Hilbert transform operator
$\Re\{\bullet\}$, $\Im\{\bullet\}$	real and imaginary part
pv	Cauchy principal value
$\mathrm{sgn}(\bullet)$	sign function
ANN	Artificial Neural Network

FORSE	FOrced Response SuitE
FRF	Frequency Response Function
MDOF	Multi Degree Of Freedom
PCA	Principal Component Analysis
PCS	Principal Component Scores
SDOF	Single Degree Of Freedom

1. Introduction

In recent years, as a result of the wide applicability of well-developed modal testing, the research focus in structural dynamics has turned to the identification of non-linear systems. Non-linear system identification is usually divided into three stages - detection, characterization and parameter quantification [1]. Detection, which aims to find non-linear behaviour in a system response, is the first step toward establishing a structural model with a good predictive accuracy. The purpose of characterization is to specify the type, spatial location and mathematical form of the non-linearities which have been detected in the structure. It is very important to detect and characterize the non-linear elastic and dissipative mechanisms involved prior to parameter quantification. Without a precise understanding of non-linear behaviour, the identification process is bound to fail [2].

A number of different approaches for detection and characterization has been developed in recent decades [2–4]. Many of these approaches are based on the violation of basic linear principles, for instance the widely used homogeneity method [5], or on the distortion of frequency response functions (FRFs) [1] or describing function inversion [6]. Such methods usually require the time-consuming measurement process of many FRFs while relying on an experienced operator to detect and characterize non-linear behaviour correctly. In addition, measured noise in FRFs frequently causes significant problems, leading to the inapplicability of some techniques [7].

The Hilbert transform is a well-known technique used in many fields of engineering, especially in signal processing [8]. Although most of its applications are performed in the time domain, the Hilbert transform can also be applied in the frequency domain. Not only does the Hilbert transform provide a fast and effective means of detecting non-linear behaviour on the basis of a measured FRF [5, 9], but it also provides limited insight into the type of non-linearities [1, 2].

However, the Hilbert transform still has several limitations. Perhaps the main limitation, which is also associated with all detection methods that look for distortion in measured signals, is the lack of an established methodology to determine if the deviations observed in an FRF are statistically significant. Therefore, the diagnosis of non-linearity requires expert judgement [2]. This limitation can be overcome by using artificial neural networks (ANNs) as suggested in [10, 11]. The approach proposed in [10] allows localization and characterization of the type of non-linearity, but it requires a full spatial model of the structure with all possible combinations of non-linearities. Unfortunately, this makes the approach difficult to use in practical applications. In contrast, the method proposed in [11] does not require the spacial model of the structure for characterization of the type of non-linearity. It uses the gain of FRFs as training data for ANNs and therefore a large number of training cases is required, while the complex nature of FRFs is not fully taken into account due to missing phase information.

A similar method as in [11] has been used in this study. In order to avoid the need for a vast set of training data, non-linearity indexes which describe the difference between an FRF and its Hilbert transform have been proposed. These indexes allow the reduction from the FRF measured in many frequency points into a set of several scalar parameters. In addition, principal component analysis may be applied for further dimensionality reduction so that the structure of the network may eventually be very compact, whilst capturing the non-linear distortion of the FRF fully. In contrast to [10], the method proposed does not require any spatial model of the structure or any a priori knowledge of the type of non-linearity.

The first part of the paper gives an overview of the techniques involved and, most importantly, introduces the non-linearity indexes. In section 3, the implementation of the method is shown in detail. Subsequently, the method is tested in section 4. Firstly, it is applied to SDOF system numerical test cases for which

robustness against measured noise is evaluated. Secondly, a cantilever plate with a localized geometric non-linearity is investigated. Section 5 demonstrates the application of the method on two experimental test rigs - a cantilever beam with a clearance, and an under-platform damper experimental rig. Based on the observations from these test cases the advantages and disadvantages of the proposed method are summarized in the conclusion.

2. A method for detection and characterization of structural non-linearities

The proposed method can be implemented in several steps. Firstly, the Hilbert transform of a frequency response function is computed. Then the difference between the FRF and its Hilbert transform is quantified using a set of scalar parameters called non-linearity indexes. The feature space created by these indexes is reduced using principal component analysis and subsequently used as the input of an artificial neural network pattern recognition algorithm by which a decision about the type of non-linearity is made. A description of the steps that are required for successful detection and characterization follows.

2.1. Normalization of frequency response functions

Initially, a frequency response function is normalized. This allows better comparison of different types of non-linearities and improves the overall performance of the introduced method. A frequency response function is transformed as follows

$$f \longrightarrow [0, 1]\,, \tag{1}$$

and

$$\|H(\omega)\| = 1, \tag{2}$$

where f is a measured frequency range, which is transformed into interval $[0, 1]$, and $H(\omega)$ is a frequency response function, which Euclidean norm $\|\bullet\|$ is to be unity. In following sections, normalized data are marked with an upper asterisk *. This normalization is possible because the absolute values of amplitudes and frequencies are not important for detection and characterization although they would be crucial for quantification. The important factor is the shape of the FRF distortion, which remains unchanged by the normalization.

To illustrate the normalization an example of two non-linear frequency response functions is shown in Fig. 1. It can be seen that the FRFs, which were significantly different in the amplitudes and frequencies,

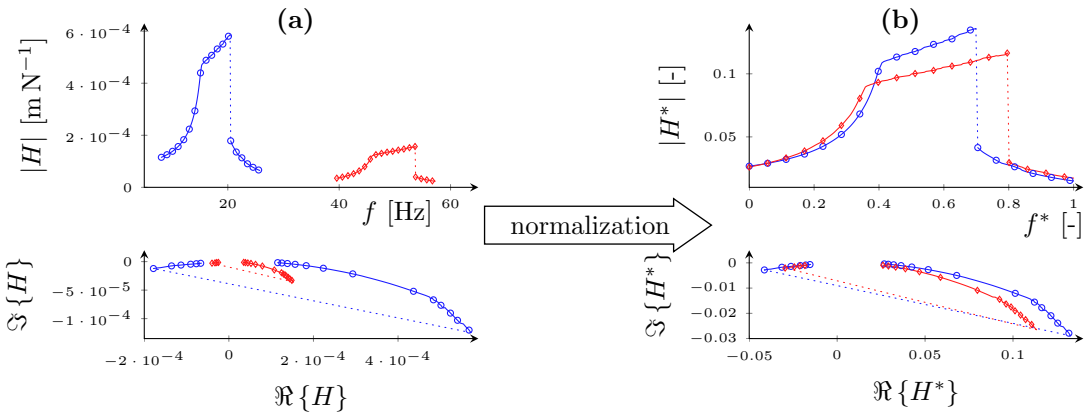

Figure 1: Normalization of two frequency response functions obtained from SDOF systems with clearance non-linearities: (a) original FRFs (b) normalized FRFs

are now much more comparable, yet they have retained the original shape.

2.2. The Hilbert transform in the frequency domain

The Hilbert transform is an integral transform from the same family as the Fourier transform. For a general complex function in the frequency domain it is defined as [1]

$$\mathscr{H}\{H(\omega)\} = \tilde{H}(\omega) = \frac{-1}{\mathrm{i}\pi}\mathrm{pv}\int_{-\infty}^{\infty}\frac{H(\Omega)}{\Omega-\omega}\mathrm{d}\Omega, \tag{3}$$

where $\mathscr{H}\{\bullet\}$ denotes the Hilbert transform operator, ω marks an angular frequency, $\tilde{H}(\omega)$ stands for the Hilbert transformed frequency response function $H(\omega)$ and "pv" denotes the Cauchy principal value of the integral. In contrast to the Fourier transform, which transforms time domain data into the frequency domain and vice versa, the Hilbert transform maps functions from a domain into the same domain by shifting their phases by $-\pi/2$ [8]. Unfortunately, analytical methods for solving Eq. (3) are not generally applicable because $H(\omega)$ cannot be found as a closed-form expression. Hence, the Hilbert transform is computed numerically either by a direct method using the Kronig-Kramers relations [12] or by means of the fast Fourier transform using an analytic signal theory [1].

It was shown in [13] that the Hilbert transform of a frequency response function can be used to detect non-linearity using the following criterion

$$\mathscr{H}\{H(\omega)\} = H(\omega) \longrightarrow \text{linear system},$$

$$\mathscr{H}\{H(\omega)\} \neq H(\omega) \longrightarrow \text{non-linear system},$$

which means that the FRF of a linear system is not affected by the Hilbert transform whereas the Hilbert transform of the FRF of a non-linear system will yield a distorted version of the original FRF. Moreover, it was observed [12] that the form of this distortion can provide some insight into the type of non-linearity.

The Hilbert transform is a fast and effective approach for detection and characterization of the type of non-linearity. Compared to the homogeneity method, the Hilbert transform can be applied on a single frequency response function which has been measured using a single excitation level [2]. In addition, the Hilbert transform does not require a linear FRF or a spatial model of the structure. As mentioned previously, a subjective decision has to be taken to detect and characterize non-linear behaviour. In order to simplify this decision a set of parameters, called non-linearity indexes, which describe the difference between an FRF and its Hilbert transform has been proposed.

2.3. Non-linearity indexes

In the scope of this study, a non-linearity index (NLI) has been defined as a real scalar parameter that describes the difference between a frequency response function and its Hilbert transform. Such index is equal to zero if the system is linear and non-zero (either positive or negative) for a non-linear system. A total number of 14 non-linearity indexes will be presented and discussed in this section. These indexes ensure the comprehensive capture of a wide range of non-linearities.

2.3.1. Correlation coefficient

Cross-correlation is commonly used as a measure of similarities between two series as the function of a lag between these series. The application of cross-correlation in the frequency domain for detection of non-linearities was proposed and demonstrated in [5]. The cross-correlation computed around a single vibration mode $R_{H\tilde{H}}(\Delta\omega)$ between a frequency response function $H(\omega)$ and its Hilbert transform $\tilde{H}(\omega)$ is defined as

$$R_{H\tilde{H}}(\Delta\omega) = \int_{\omega_{\min}}^{\omega_{\max}} H(\omega)\tilde{H}(\omega+\Delta\omega)\mathrm{d}\omega, \tag{4}$$

where $\Delta\omega$ is a frequency shift (lag), and $\omega_{\min}$ and $\omega_{\max}$ are the lower and upper integral limits respectively. These limits have to be chosen appropriately to capture the distortion of an FRF; as a convention [1], the half-power points that solve the following equation

$$|H(\omega)| - \frac{\max|H(\omega)|}{\sqrt{2}} = 0 \tag{5}$$

are used. Alternatively, in a scheme of detection and characterization, other limits could be taken as long as they describe the distortion of an FRF. In addition, Eq. (4) and all following integrals have to be solved approximately using numerical approaches since analytical expressions for $H(\omega)$ and $\tilde{H}(\omega)$ are not generally known.

The first non-linearity index (NLI_1) is defined based on the squared cross-correlation coefficient at the frequency shift $\Delta\omega = 0$ using the following expression

$$\mathrm{NLI}_1 = 1 - \|R_{H\tilde{H}}(0)\|^2. \tag{6}$$

Due to its definition, this index is more sensitive to non-linearities that shift the resonance frequency, such as geometric non-linearities, and less sensitive to non-linearities that scale the amplitudes of FRFs, for instance non-linear damping.

2.3.2. Hilbert transform describers

It was proven in [12] that all spectral moments exist for an FRF as well as its Hilbert transform. These moments are defined as

$$M_H^{(n)} = \int_{\omega_{\min}}^{\omega_{\max}} \omega^n H(\omega)\mathrm{d}\omega, \tag{7}$$

where $M_H^{(n)}$ stands for the nth-order spectral moment of a frequency response function $H(\omega)$. In spite of the fact that these moments are complex, they can be considered as an analogy with statistical theory, where the first- and second-order moments measure the mean and the standard deviation of a probability distribution. The third- and fourth-order moments describe the skewness and kurtosis [1] and the zeroth-order moment can be viewed as the area under the complex function. For the purpose of description of non-linearity, relative differences are defined between the spectral moments of an FRF $M_H^{(n)}$ and moments of its Hilbert transform $M_{\tilde{H}}^{(n)}$. These parameters are called Hilbert transform describers ($\mathrm{HTD}^{(n)}$) [1]

$$\mathrm{HTD}^{(n)} = \frac{M_{\tilde{H}}^{(n)} - M_H^{(n)}}{M_H^{(n)}}. \tag{8}$$

Although an arbitrary number of HTDs can be computed, the first three (zeroth-, first- and second-order) are considered in this study. The non-linearity indexes were defined as the real and imaginary part of the Hilbert transform describers, i.e.

$$\mathrm{NLI}_2 = \Re\left\{\mathrm{HTD}^{(0)}\right\}, \qquad \mathrm{NLI}_3 = \Im\left\{\mathrm{HTD}^{(0)}\right\}. \tag{9}$$

In a similar manner $\mathrm{NLI}_{4,5}$ and $\mathrm{NLI}_{6,7}$ were defined, but $\mathrm{HTD}^{(1)}$ and $\mathrm{HTD}^{(2)}$ were used instead. The imaginary parts of the HTD, by extension NLI_3, NLI_5 and NLI_7, separate the stiffness hardening and softening very well. On the other hand, the real parts of the HTDs effectively distinguish between the quadratic damping and dry friction. An example of this behaviour will be shown in Fig. 4.

2.3.3. Function describers

To describe relative changes between an FRF and its Hilbert transform, it is proposed to compute some parameters that are used in classic mechanics. First of which, the centre of gravity of an FRF, γ_1 can be

calculated as

$$\gamma_1 = \frac{\int\limits_{\omega_{\min}}^{\omega_{\max}} m(\omega) H(\omega) \mathrm{d}\omega}{\int\limits_{\omega_{\min}}^{\omega_{\max}} m(\omega) \mathrm{d}\omega}, \tag{10}$$

where $m(\omega)$ would be the length density in mechanics. Here, it can be set as unity or the coherence function can be used if available. If the coherence was employed, non-linear effects of the resonance frequencies would be emphasized. The non-linearity indexes derived from the centre of gravity are assembled as the relative difference between the FRF γ_1 and its Hilbert transform $\tilde{\gamma}_1$ and by splitting this value into the real and imaginary part

$$\mathrm{NLI}_8 = \Re\left\{\frac{\tilde{\gamma_1} - \gamma_1}{\gamma_1}\right\}, \qquad \mathrm{NLI}_9 = \Im\left\{\frac{\tilde{\gamma_1} - \gamma_1}{\gamma_1}\right\}. \tag{11}$$

These non-linearity indexes can particularly distinguish between stiffness and damping non-linearities as the Hilbert transform of the FRFs with damping non-linearities usually scales the FRFs and therefore does not change the position of the centre of gravity significantly.

Other parameters have been introduced to describe complex curve properties based on mechanical analogies, namely the moment of inertia about ω-axis γ_2 and with respect to origin γ_3 defined as

$$\gamma_2 = \int\limits_{\omega_{\min}}^{\omega_{\max}} m(\omega) \left(\Re\{H(\omega)\}^2 + \Im\{H(\omega)\}^2\right) \mathrm{d}\omega, \tag{12}$$

and

$$\gamma_3 = \int\limits_{\omega_{\min}}^{\omega_{\max}} m(\omega) \left((\omega - \overline{\omega})^2 + \Re\{H(\omega) - \gamma_1\}^2 + \Im\{H(\omega) - \gamma_1\}^2\right) \mathrm{d}\omega, \tag{13}$$

where $\overline{\omega}$ marks the mean of angular frequency. These moments can be interpreted as the torque needed for an unity angular acceleration about the ω-axis or the origin. These parameters are real so their relative difference creates other non-linearity indexes

$$\mathrm{NLI}_{10} = \frac{\tilde{\gamma_2} - \gamma_2}{\gamma_2}, \qquad \mathrm{NLI}_{11} = \frac{\tilde{\gamma_3} - \gamma_3}{\gamma_3}, \tag{14}$$

where $\tilde{\bullet}$ marks the entities which have been computed from the Hilbert transform of an FRF. Again, the parameters are significantly higher for stiffness non-linearities as the Hilbert transform shifts the frequencies of such non-linearities and therefore changes the moments of inertia significantly.

2.3.4. Statistical description

Other non-linearity indexes can be assembled directly from the complex difference between an FRF and its Hilbert transform

$$G(\omega) = \tilde{H}(\omega) - H(\omega). \tag{15}$$

This difference $G(\omega)$ can be described in terms of describing statistics. The mean of the difference is defined as

$$\overline{G} = \frac{1}{\mathrm{n_{sl}}} \sum_{k=1}^{\mathrm{n_{sl}}} G(\omega_k), \tag{16}$$

where $\mathrm{n_{sl}}$ is a number of spectral lines between $\omega_{\min}$ and $\omega_{\max}$. Two non-linearity indexes $\mathrm{NLI}_{12,13}$ are then obtained by splitting this complex mean into real and imaginary parts.

The last proposed non-linearity index is formed using the standard deviation of the difference $G(\omega)$

$$\mathrm{NLI}_{14} = \sigma = \sqrt{\frac{1}{\mathrm{n_{sl}} - 1} \sum_{k=1}^{\mathrm{n_{sl}}} (G(\omega_k) - \overline{G})^2}, \tag{17}$$

which describes an amount of variation or dispersion of $G(\omega)$ about the mean $\overline{G}$.

Fourteen non-linearity indexes have been presented in this section and are summarized in Tab. A.1. Most of them have an integral form so that they are robust to measured noise and other errors which can occur in an FRF. However, all of them depend on the integration limits $\omega_{\min}$ and $\omega_{\max}$. Although the choice of these limits affects the absolute value of the non-linearity indexes, it is not a major issue as long as these limits are consistent for all computed non-linearity indexes. Generally, the half-power points should be chosen. If they cannot be defined due to, for example, a jump in an FRF, the part of an FRF which covers the non-linear distortion should be taken. It should be also noted that for the indexes to be meaningful, and the method to work correctly, the modes should be well separated and no non-linear coupling should exist between them.

It was observed [1, 12] that the distortion of an FRF and also its Hilbert transform is unique for a given type of non-linearity. Therefore, the pattern created by the non-linearity indexes is also unique and suitable as the input of a pattern recognition algorithm. Artificial neural networks have been chosen as the pattern recognition algorithm in this study. With regards to the feature of neural networks to grow exponentially with a number of the input parameters [14], a number of the non-linearity indexes is further reduced using principal component analysis.

2.4. Principal component analysis

Principal component analysis (PCA), also known as Karhunem-Loève transform or proper orthogonal decomposition [15], seeks a linear projection of high-dimensional data into lower dimensional space in a least-squares sense [16]. The principal component analysis projects the initial n-dimensional data vector of samples (observations) $\mathbf{x}_s = (x_1, \ldots, x_n)^T$ into a new n-dimensional vector $\mathbf{z} = (z_1, \ldots, z_n)^T$ called the principal component scores (PCS). The new coordinates have the following properties: z_1 is the linear combination of the original x_i with maximum possible variance, z_2 is the linear combination which explains most of the remaining variance and is orthogonal to z_1 and so on [14].

The principal component algorithm can be summarized in following steps: for a set of observations $\{\mathbf{x}_1, \ldots, \mathbf{x}_N\}$ the scatter matrix $\mathbf{S}$ is assembled using

$$\mathbf{S} = \sum_{k=1}^{N} (\mathbf{x}_i - \overline{\mathbf{x}})(\mathbf{x}_i - \overline{\mathbf{x}})^T, \tag{18}$$

where $\overline{\mathbf{x}}$ is a vector of sample means. Then the scatter matrix $\mathbf{S}$ is decomposed (usually using singular value decomposition)

$$\mathbf{S} = \mathbf{U}\mathbf{\Sigma}\mathbf{V}^T, \tag{19}$$

where $\mathbf{\Sigma}$ is a diagonal matrix interpreted as the relative contributions of the principal scores to the total variance and $\mathbf{U}$ is an orthonormal matrix which contains the principal directions. Subsequently, the principal component scores are obtained from

$$\mathbf{z}_i = \mathbf{U}^T(\mathbf{x}_i - \overline{\mathbf{x}}). \tag{20}$$

Dimensionality reduction is then achieved by selecting only those principal component scores which contribute significantly to the overall variance and therefore retain the dominant information of the data. While the principal component analysis is a linear transformation, it cannot remove non-linear correlations within data sets.

The linear principal component scores are used as the inputs of the neural network. The dimension of the problem can be significantly reduced using the PCA as will be shown later.

2.5. Artificial neural networks

Artificial neural networks, which belong to a group of soft or natural computing methods, have been applied to many problems in recent years. In mechanical engineering applications they are usually used for classification, detection of abnormalities and input-output mapping [14]. Although many types of artificial neural networks can be found in literature, a multi-layer perception neural network is usually applied for pattern recognition tasks. Moreover, only a single hidden layer is often used as it was proven that such network can approximate an arbitrary problem [16].

The multi-layer perception network has nodes and neurons arranged in layers that are passed by a signal from the input layer, through hidden layer(s), into the output layer. A weighted sum $w_{ij}^{(k)}$ of all signals $x_i^{(k-1)}$ at each node i in layer $k-1$ is passed through an activation (or transfer) function $f(x)$ to the node $x_j^{(k)}$ of the following layer

$$x_i^{(k)} = f\left(\sum_j w_{ij}^{(k)} x_j^{(k-1)}\right). \tag{21}$$

The choice of the activation function $f(x)$ depends on the application [17]. For pattern recognition, the hyperbolic tangent function is used in the hidden layer(s) and a non-linear activation function is used for the output layer. So called softmax activation is often used as the non-linear activation function because it forces the output of the network to sum to unity and therefore provides a condition for interpreting the outputs as the probabilities of classes.

The first stage when applying the artificial neural network is to establish the appropriate values for the weights w_{ij}. This stage is referred to as the training phase in which the network is presented by a set of the input parameters and the corresponding outputs. At each training step the inputs are passed through the network yielding trial outputs that are compared to the desired outputs. If a significant error is found, the error is passed backwards through the network and the weights are adjusted. This is referred to as the backpropagation algorithm. This algorithm can use different update rules [17], but the scaled conjugate gradient backpropagation is usually the first choice.

One of the main problems of ANNs, and many soft computing methods, is generalisation of the network. The problem with generalization occurs when there are too many weights compared to a number of training points or patterns. The simplest solution to the problem is to always have enough data. There is no versatile technique how to choose a number of the hidden layer's neurons (and therefore a number of weights w_{ij}) before training, but some guidelines have been established based on the practical experience and can be found in [16].

2.6. Summary of the proposed method

The method is summarized in the flow chart in Fig. 2 in which two branches are distinguished. Although they look very similar, there is a major difference between them. The preparation of the neural network can be performed only once to train it and subsequently this network can be used multiple times. However, the preparation is a time-consuming process, mainly because of the need for relevant training data, which can be computed or experimentally measured. Once the neural network has been trained, non-linear behaviour can be detected and characterized from a single frequency response function in a timely fashion.

The method operates on a single mode of vibration. Therefore, when applied to a MDOF system the modes are treated separately as having been obtained from a SDOF system. It implies that for the method to work correctly the modes must be well-separated, with no significant linear or non-linear coupling.

In certain situations, there might co-exist several non-linear elastic and dissipative mechanisms in the structure, such as dry friction and geometric non-linearities. The method proposed does not provide any reliable information about how many or what combinations of non-linearities are present in the system. As the superposition principle is not valid for non-linear systems [1] the combination of non-linearities is simply another non-linearity, and the separation of this non-linearity into two, or more, is not uniquely possible without a priori knowledge of the system. Yet, if the neural network has been trained for certain types of non-linearities, some limited insight into the combination of the types involved can be given due to the capability of ANNs to characterize unseen patterns. An example of this capability is shown in section 5.2.

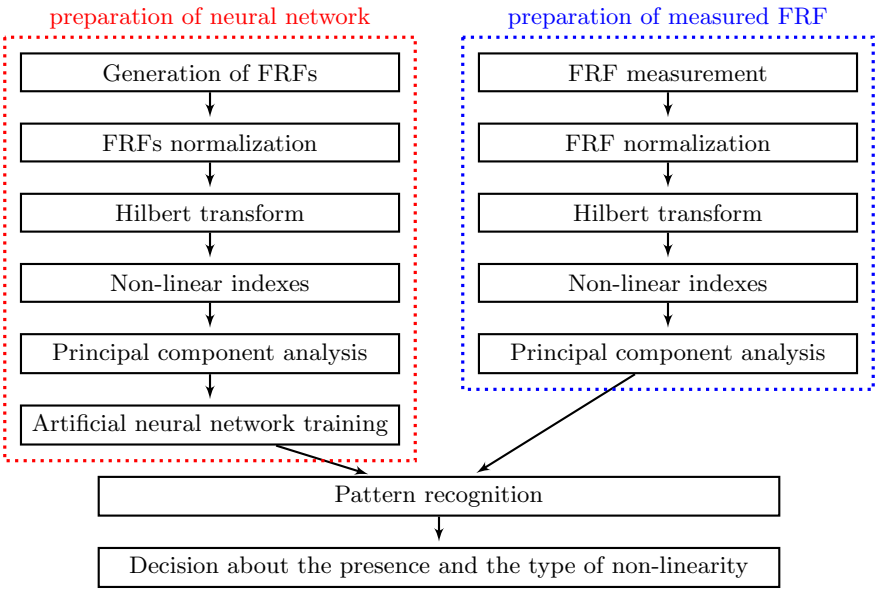

Figure 2: Summary of the proposed method for detection and characterization of non-linearities

3. Implementation of the method

Although the method could be used for an arbitrary number of non-linearities, just a limited number was considered in this study, namely cubic hardening stiffness, cubic softening stiffness, clearance, Coulomb friction and non-linear (quadratic) damping. In addition, the linear system was added into this set. The method was implemented according to Fig. 2.

3.1. Training data calculation

The training data for ANNs were obtained numerically for a linear SDOF system and SDOF systems with the mentioned types of non-linearities. Such systems are described using the equation of motion

$$m\ddot{x} + c\dot{x} + kx + g_{\mathrm{nl}}(x, \dot{x}) = F(t), \tag{22}$$

where m is a mass, c is a linear damping coefficient, k is a linear stiffness coefficient, $F(t)$ is the excitation force and $x, \dot{x}, \ddot{x}$ are displacement, velocity and acceleration, respectively. The term $g_{\mathrm{nl}}(x, \dot{x})$ describes a non-linear force. It is, therefore, zero for a linear system and varies with the type of the non-linearity involved (see Tab. 1).

In order to obtain the frequency response functions of the non-linear systems, an experimental approach called stepped sine excitation measurement was implemented in a numerical simulation. The system is excited by a single frequency sine wave, the time domain output is computed using the direct integration of Eq. (22) using Matlab (`ode45`) function, and a single point of an FRF is extracted using a frequency response analyser [18]. The process is repeated for all frequencies of interest. The approach is computationally expensive, but provides the data in an equivalent form to expected experimental measurements.

For each type of non-linearity frequency response functions were generated with the parameters of the systems randomly chosen from the ranges shown in Tab. 1. The FRFs were calculated in 256 frequency lines distributed symmetrically around the undamped natural resonance $f_0 = \sqrt{k/m}/2\pi$ with the frequency resolution $\Delta f = 0.1$ Hz. For all systems the stepped sine excitation with the increasing excitation frequency was used with exception of the system with the cubic softening stiffness where a decreasing rate was employed. The excitation amplitude was randomly selected from interval $F = [0.1, 2]$ N. Eventually, 500 FRFs of each system were calculated (this number will be justified in section 3.5).

Non-linearity	$g_{\mathrm{nl}}(x,\dot{x})$	Parameters range
Linear system	0	$m = 1$ kg ; $k = \left[7\times10^3, 5\times10^5\right]$ N m^{-1}
		$c = \alpha m + \beta k$ N m^{-1} s^{-1}; $\alpha = [2,5]$; $\beta = \left[10^{-8}, 10^{-6}\right]$
Cubic stiffness, hardening	$k_{\mathrm{nl}}x^3$	$k_{\mathrm{nl}} = \left[5\times10^3 k, 5\times10^4 k\right]$ N m^{-3}
Cubic stiffness, softening	$k_{\mathrm{nl}}x^3$	$k_{\mathrm{nl}} = \left[-5\times10^3 k, -5\times10^4 k\right]$ N m^{-3}
Clearance	$k_{\mathrm{nl}}x - k_{\mathrm{nl}}b, \quad x > b$	$k_{\mathrm{nl}} = [1k, 10k]$ N m^{-1}
	$0, \quad \lvert x\rvert < b$	$b = [0.1, 0.5]$ mm
	$k_{\mathrm{nl}}x + k_{\mathrm{nl}}b, \quad x < -b$	
Coulomb friction	$\mu N_{\mathrm{f}}\mathrm{sgn}(\dot{x})$	$\mu N_{\mathrm{f}} = [0.05, 0.2]$ N
Quadratic damping	$c_{\mathrm{nl}}\dot{x}\lvert\dot{x}\rvert$	$c_{\mathrm{nl}} = [10c, 50c]$ N m^{-2} s^{-1}

Table 1: Non-linear force and parameter ranges for SDOF non-linear systems used for the calculation of the training data

The parameters and excitation amplitude of the system were chosen in such a manner that the distortion of the calculated FRFs was similar to the distortion observed during experimental measurements. To illustrate the distortion and the frequency resolution, normalized FRFs for each type with weak, moderate and strong non-linear effects are displayed in Fig. 3.

3.2. Hilbert transform in the frequency domain

The direct approach was used for the calculation of the Hilbert transform. This approach suffers from truncation errors as explained in [12]. However, due to the normalization these errors are minimized. The Hilbert transform of the cases considered is also displayed in Fig. 3.

3.3. Non-linearity indexes

For the evaluation of the non-linearity indexes the half-power points were used and $m(\omega)$ in Eqs. (10), (11) and (12) set to unity. The non-linearity indexes were subsequently checked using box plots. The purpose of this process was to observe if there is no strong overlap, or in other words, if linear and non-linear systems do not produce the same values. If this was the case, the NLI would be discarded because it would not bring new information into the process and it could possibly decrease the quality of the pattern. An example of such box plots for 3 NLIs can be seen in Fig. 4.

The non-linearity index derived from the correlation coefficient is displayed in Fig. 4a from which the ability to distinguish between stiffness and damping non-linearities can be observed. While cubic hardening, softening and clearance produce significantly higher values of this index, quadratic damping, Coulomb friction and linear systems are very close to zero. The non-linearity indexes that have been calculated based on the 1st-order Hilbert transform describers are shown in Fig. 4b and Fig. 4c. Similarly to the correlation coefficient, the values of these indexes differ for each type of non-linearity although some overlap can be observed. The NLI_4 effectively distinguishes between Coulomb friction and quadratic damping and the NLI_5 between hardening and softening stiffness.

It is clear that the non-linear indexes significantly reduce the dimension of the pattern recognition problem. Starting from the complex frequency response functions, which have been evaluated in 265 frequency points, the problem has been reduced into 14 scalar parameters that represent the different types of non-linearities.

3.4. Principal component analysis

Principal component analysis was applied for further reduction of the dimensionality in order to reduce a number of the input parameters for the ANN as much as possible. Using the procedure described in section 2.4 it was found that only 3 principal components are needed for capturing just over 95 % of the total variance (see Fig. 5a). Therefore, only a set of the first three principal component scores is needed to classify the pattern. Moreover, these three components can be plotted using three dimensional space.

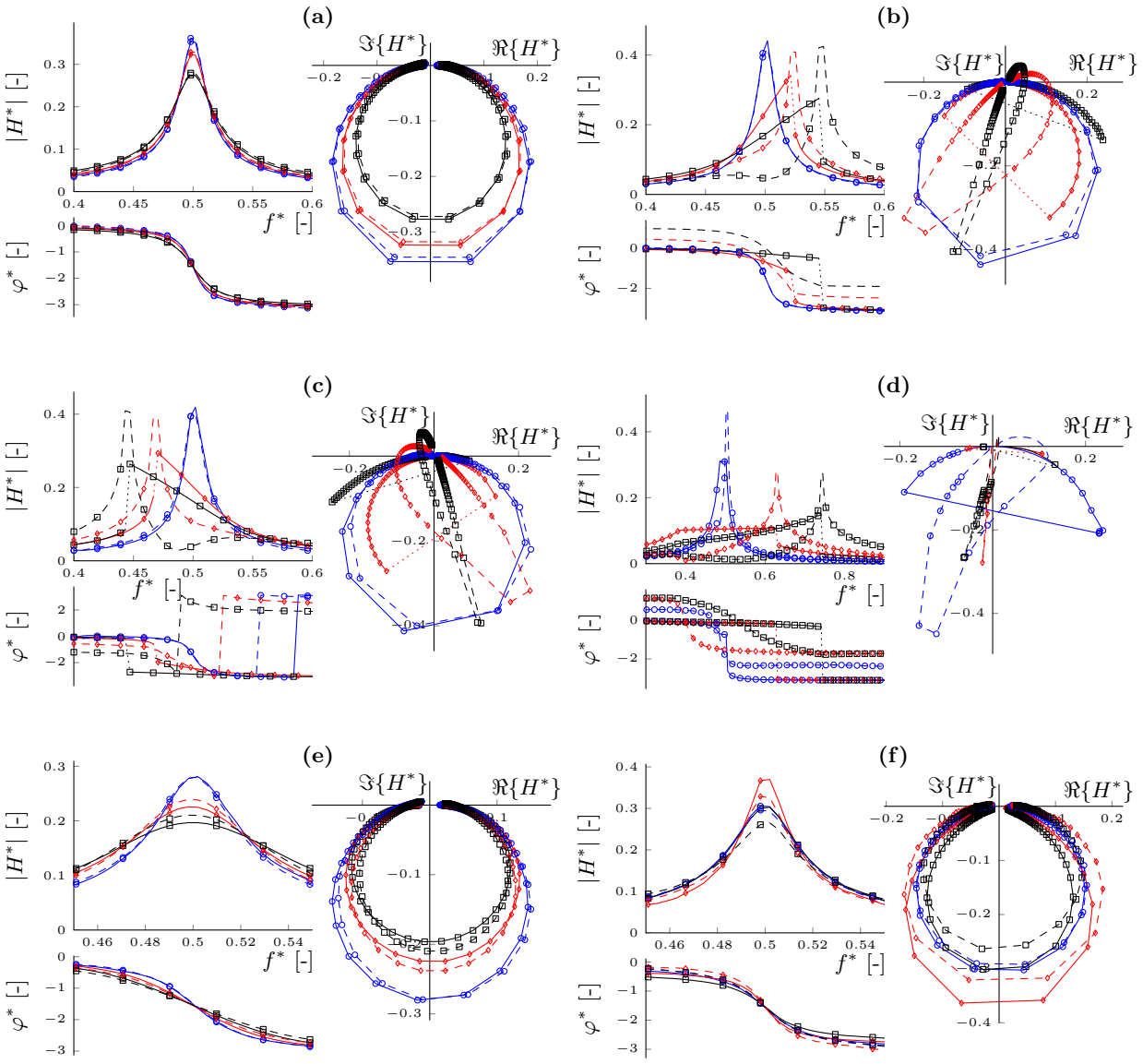

Figure 3: Frequency response functions (solid line) and their Hilbert transform (dashed line) of (a) linear (b) cubic hardening stiffness (c) cubic softening stiffness (d) clearance (e) non-linear (quadratic) damping (f) Coulomb friction system with the weak (blue circles), moderate (red diamonds) and strong (black squares) non-linear distortion

As can be seen in Fig. 5b the three principal components well separate the groups of the considered non-linear systems. In addition, such a plot allows direct classification of a new pattern by evaluating the position of the new principal component score in the graph. This technique will be demonstrated on experimentally obtained FRFs in section 5.

3.5. Artificial neural network

The principal component scores were used as the input data of the artificial neural network and the output classes were defined by the types of non-linearities. Therefore, the neural network has 3 inputs nodes, 6 output nodes and a single hidden layer. A number of the nodes in the hidden layer was found using the 1 to M training strategy [14], leading to 4 nodes in this layer. The final network has the structure 3:4:6 hence

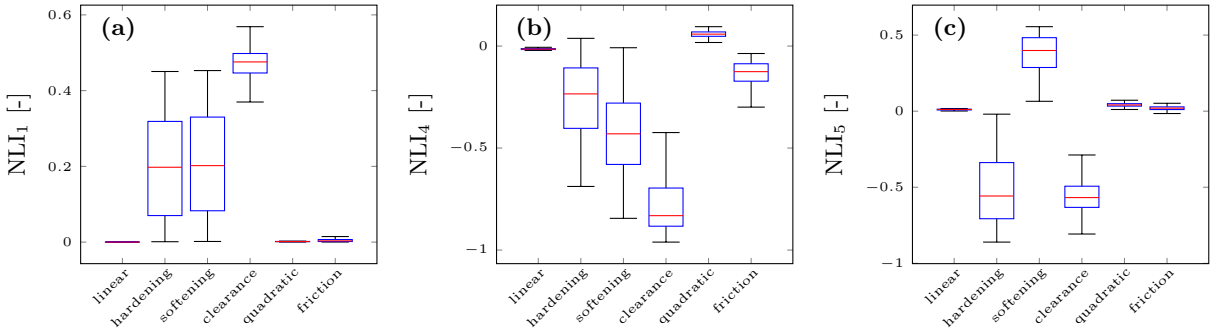

Figure 4: Box plots: (a) NLI_1 - correlation coefficient, (b) NLI_4 - real part of 1st-order HTD, (c) NLI_5 - imaginary part of 1st-order HTD

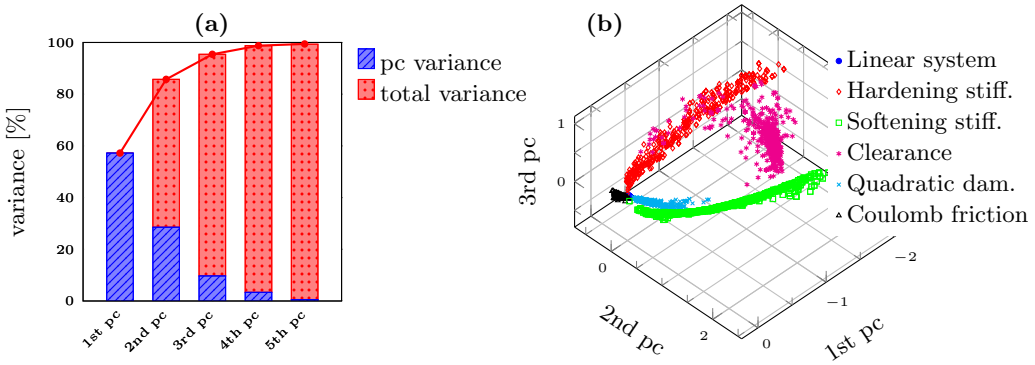

Figure 5: Principal component analysis: (a) variance captured by principal components, (b) principal component scores

possesses 46 weights. Therefore, 500 training FRFs for each non-linearity were used which corresponds with one of the "rule of thumb" which says that at least 10 times more data are required for good generalization of unseen patterns [14]. The network was implemented using the Neural Network Matlab toolbox.

Once the network had been trained, it was presented with all 500 systems for each non-linearity as the testing data. The so-called confusion matrix of this testing is shown in Tab. 2. Nearly all cases were identified

Classified class	Desired class					
	1.	2.	3.	4.	5.	6.
1. Linear system	500/100 %	0	0	0	0	1/0.2 %
2. Hardening stiffness	0	499/99.8 %	0	17/3.4 %	0	0
3. Softening stiffness	0	0	499/99.8 %	0	0	0
4. Clearance	0	1/0.2 %	0	482/96.4 %	0	0
5. Quadratic damping	0	0	1/0.2 %	1/0.2 %	500/100 %	0
6. Coulomb friction	0	0	0	0	0	499/99.8 %

Table 2: Testing confusion matrix

correctly and only a low percentage of confusion can be seen for the systems with the clearance non-linearity. Some of these cases were misclassified as the hardening stiffness. This, however, is understandable as the physical mechanism of these two non-linearities is similar.

4. Application on numerical examples

4.1. Application on noisy SDOF systems

In order to evaluate the robustness of the method against measured noise, the method was applied to white-noise polluted frequency response functions. Different levels of noise were introduced to all 500 FRFs for each non-linearity with the signal to noise ratio of 25, 20 and 15 dB (see Fig. 6).

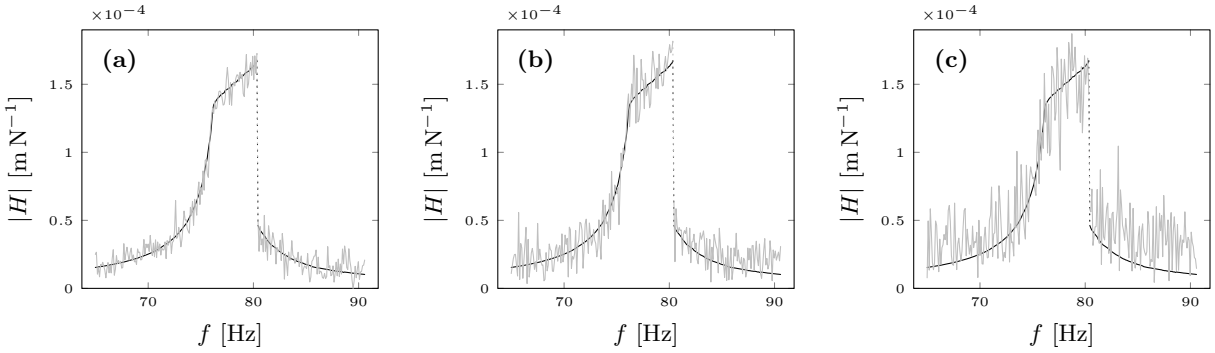

Figure 6: FRFs of the system with the clearance non-linearity without noise (black) and polluted by noise (grey) with signal-to-noise ratio (a) 25 dB, (b) 20 dB, (c) 15 dB

When testing the robustness against noise, the class with the highest network output (the highest probability) was taken as the identified class. The results of the classification are summarized in Tab. 3, 4 and 5 in which the percentage does not refer to the probability of an output class, but it is a percentage of identified systems out of 500.

Classified class	Desired class					
	1.	2.	3.	4.	5.	6.
1. Linear system	496/99.2 %	0	0	0	4/0.8 %	3/0.6 %
2. Hardening stiffness	0	497/99.4 %	0	19/3.8 %	0	0
3. Softening stiffness	0	0	499/99.8 %	1/0.2 %	0	0
4. Clearance	0	3/0.6 %	0	479/95.8 %	0	0
5. Quadratic damping	3/0.6 %	0	1/0.2 %	1/0.2 %	496/99.2 %	0
6. Coulomb friction	1/0.2 %	0	0	0	0	497/99.4 %

Table 3: Characterization results for signal-to-noise ratio 25 dB

Classified class	Desired class					
	1.	2.	3.	4.	5.	6.
1. Linear system	436/87.2 %	1/0.2 %	0	0	4/0.8 %	9/1.8 %
2. Hardening stiffness	0	487/97.4 %	0	101/20.2 %	0	0
3. Softening stiffness	0	0	496/99.2 %	10/2 %	0	0
4. Clearance	0	12/2.4 %	0	376/75.2 %	0	0
5. Quadratic damping	39/7.8 %	0	3/0.6 %	10/2 %	496/99.2 %	0
6. Coulomb friction	25/5 %	0	1/0.2 %	3/0.6 %	0	491/98.2 %

Table 4: Characterization results for signal-to-noise ratio 20 dB

It can be seen that the artificially introduced white noise influences the results of the classification. The influence is low for the highest signal-to-ratio and becomes significant for higher amount of noise. However,

Classified class	Desired class					
	1.	2.	3.	4.	5.	6.
1. Linear system	342/68.4 %	1/0.2 %	0	0	16/3.2 %	18/3.6 %
2. Hardening stiffness	12/2.4 %	472/94.4 %	0	215/43 %	2/0.4 %	1/0.2 %
3. Softening stiffness	2/0.4 %	0	491/94.2 %	32/6.4 %	2/0.4 %	2/0.4 %
4. Clearance	0	27/5.4 %	0	213/42.6 %	0	0
5. Quadratic damping	75/15 %	0	7/1.4 %	37/7.4 %	479/95.8 %	2/0.4 %
6. Coulomb friction	69/13.8 %	0	2/0.4 %	3/0.6 %	1/0.2 %	477/95.4 %

Table 5: Characterization results for signal-to-noise ratio 15 dB

despite having some misleading detection and characterization, it can be seen that a majority of systems are classified properly. The most significant problems are encountered for the clearance non-linearity under the strong influence of added noise (signal-to-noise ratio 15dB). Under this condition, just under an half of the systems is characterized properly. On the other hand, a significant portion of the systems is again characterized as the cubic hardening stiffness which is similar to clearance in terms of structural behaviour.

Significant confusion can also be observed between linear systems and systems with quadratic damping and Coulomb friction for signal-to-noise ratios lower than 20dB. Up to 30 % of systems have been classified as non-linear despite being linear, but due to the very large amount of noise (see Fig. 6c) this can still be considered as an acceptable result.

4.2. Application on a lumped parameter MDOF system

A simple model of a cantilever plate with a cubic non-linearity is used to demonstrate the performance of the methodology on MDOF systems. The model shown in Fig. 7 consists of 15 discrete masses ($m = 1$ kg) which are connected via linear springs ($k = 1 \times 10^6$ N m^{-1}). The viscous damping is introduced using Rayleigh's proportional damping model ($\alpha = 2$; $\beta = 1 \times 10^{-8}$). The plate is fixed at two edges and free at the other two. The system is excited by a sinusoidal force $F(t)$ that is placed in the corner of the plate and pointed in x-direction while the plate is allowed to vibrate only in this direction. Two amplitudes of the excitation force are chosen ($F = 10$ N; $F = 20$ N) to emphasize the effect of the non-linearity. The non-linear spring with cubic hardening behaviour ($k_{\mathrm{nl}} = 1 \times 10^{10}$ N m^{-3}) is placed in the same position as the excitation force.

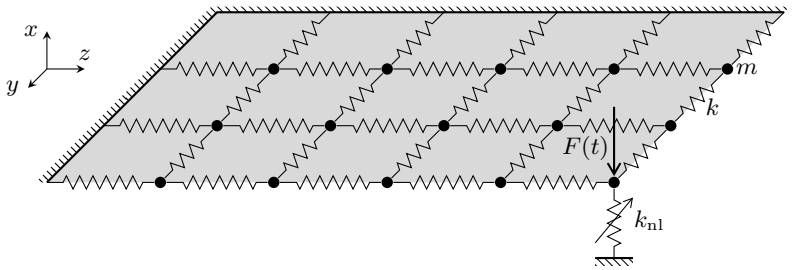

Figure 7: The model of the cantilever plate with a cubic hardening non-linear spring

The equations of motion, which were assembled using the Lagrange equations of the second kind, are written in a matrix form as

$$\mathbf{M}\ddot{\mathbf{x}} + [\alpha\mathbf{M} + \beta\mathbf{K}]\,\dot{\mathbf{x}} + \mathbf{K}\mathbf{x} + \mathbf{G}_{\mathrm{nl}}(\mathbf{x}, \dot{\mathbf{x}}) = \mathbf{F}(t), \tag{23}$$

where $\mathbf{M}$, $\mathbf{K}$ are mass and stiffness matrices; $\mathbf{x}$, $\dot{\mathbf{x}}$, $\ddot{\mathbf{x}}$ marks displacement, velocity and acceleration vectors, and $\mathbf{F}(t)$ is the excitation force vector. The term $\mathbf{G}_{\mathrm{nl}}(\mathbf{x}, \dot{\mathbf{x}})$ describes the non-linear forces. The steady state

solution of such non-linear differential equations is commonly approximated using a Fourier series

$$\mathbf{x}(t) = \mathbf{X}_0 + \sum_{j=1}^{\mathrm{n_h}} \mathbf{X}_j^c \cos(n_j \omega t) + \mathbf{X}_j^s \sin(n_j \omega t), \tag{24}$$

where $\mathbf{X}_j^c$ and $\mathbf{X}_j^s$ are the harmonic coefficients, $\mathbf{X}_0$ represents the displacement due to static forces, n_j is a number of harmonics that are used in the multi-harmonic displacement representation, $\mathrm{n_h}$ is a total number of harmonics taken into account, and ω is the excitation frequency. An in-house multi-harmonic balance solver FORSE (FOrce Response SuitE) [19], which uses an alternating frequency-time procedure [20], was used to compute the FRFs of the system. The first 3 harmonics were included in the calculation. The calculated FRFs at the position of the non-linearity can be seen in Fig. 8 where the frequency range covering the first 5 modes is shown.

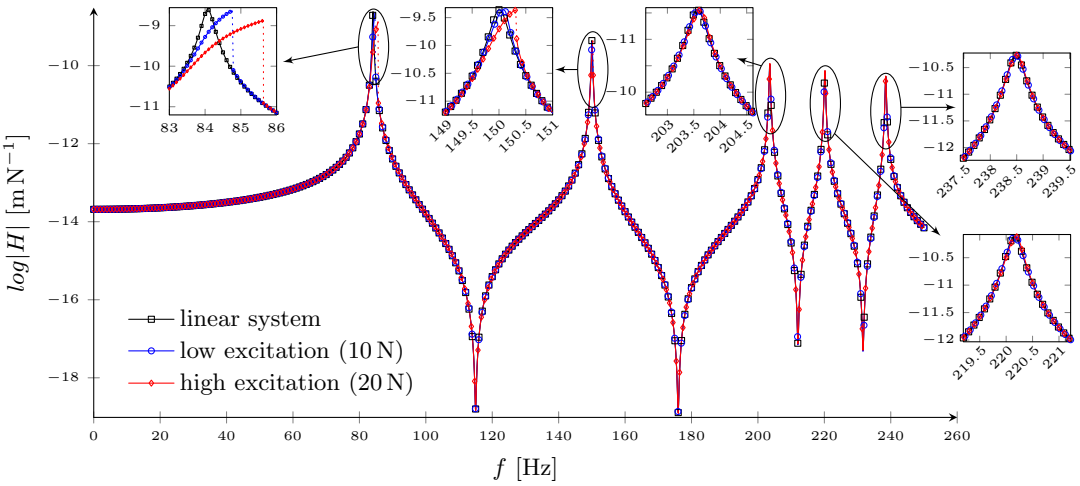

Figure 8: Frequency response functions of the lumped parameter model of the cantilever plate

For detection and characterization of non-linear behaviour, the network was exactly the same as for the previous cases, i.e. no additional training data have been added. As previously discussed, the method has to be applied on a single mode of vibration. Therefore, the multi-mode FRF was divided at the anti-resonances and the modes were treated separately as if they were obtained from a SDOF system. The results of the classification are summarized in Tab. 6 in which the percentage in the brackets indicates the probability of the classified class.

	linear	low excitation (10 N)	high excitation (20 N)
mode 1	linear (98.1 %)	hardening (98.8 %)	hardening (99.9 %)
mode 2	linear (96.0 %)	hardening (99.6 %)	hardening (93.2 %)/clearance (6 %)
mode 3	linear (97.9 %)	linear (83.3 %)/hardening (16.3 %)	hardening (98.3 %)
mode 4	linear (95.7 %)	linear (92.6 %)	linear (78.9 %)/hardening (20.7 %)
mode 5	linear (95.4 %)	linear (93.5 %)	linear (93.8 %)

Table 6: Characterization results of the lumped parameter model of the cantilever plate

It is clear that all considered modes of the linear FRF have been classified correctly, but some confusion can be observed for non-linear FRFs. However, it can be seen from the insets of modes in Fig. 8 that the non-linear distortion is very weak in higher modes. Not only has the method been able to identify strong cubic hardening behaviour in several first modes, but it also provided an indication of the appearance of weaker non-linear effects as can be seen in the 3rd mode under low excitation and in the 4th mode under

high excitation. For these modes, the network indicated about 20 % probability that the mode behaves non-linearly, which cannot be directly observed in Fig. 8. It can also be noticed in Tab. 6 that the probability of the hardening behaviour for the second mode is slightly lower for the higher excitation than the same probability for the lower excitation. This result is caused by the misclassification of the hardening behaviour as the clearance non-linearity. As discussed previously, this misclassification may be explained by similar physical mechanics of these two non-linearities.

5. Application on experimental data

The method was tested on several experimentally measured frequency response functions, which were available from previous measurements of a simple cantilever beam with a clearance non-linearity and a more complex under-platform damper experimental test rig.

5.1. Cantilever beam with a clearance non-linearity

The experimental set-up can be seen in Fig. 9a. A thin steel beam (300x36x3 mm) is held by a very stiff (considered rigid) clamp at one end and is unsupported at the another end. Large bolts allow the application of a significant clamping force to enforce linear behaviour in the clamp.

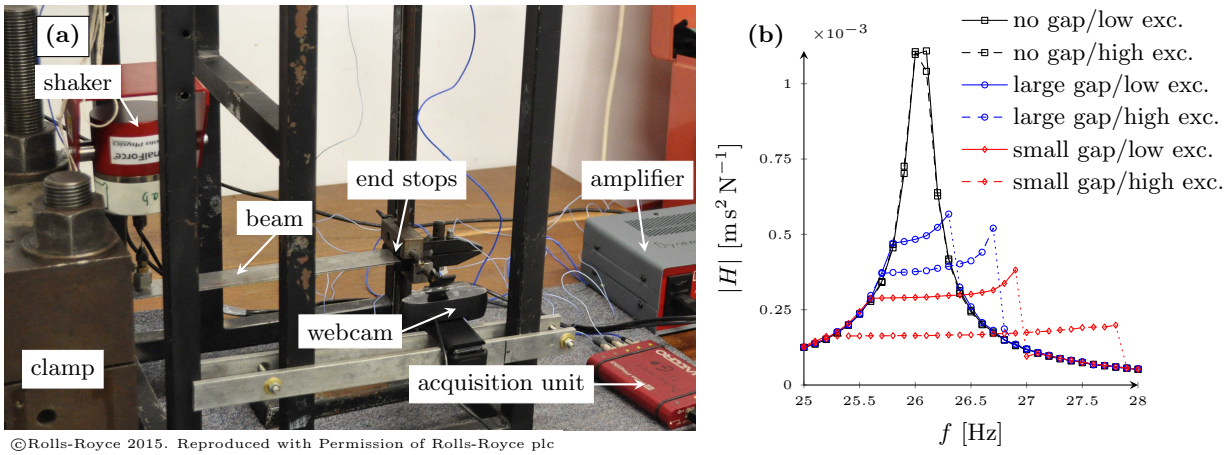

Figure 9: Cantilever beam: (a) experimental configuration (b) measured FRFs

The system is excited by a permanently attached shaker which is placed as close to the clamp as possible. An uncontrolled stepped sine excitation is used to evaluate non-linear behaviour which is ensured by an adjustable non-linearity of hardening type. Two end stops are placed close to the free end of the beam representing a backlash, which can be found in many engineering applications, including aircraft engines (e.g. blade casing interaction). The end stops are created by a smaller clamp, which is rigidly attached to the supporting bar.

As the non-linearity can be controlled through the size of the gaps the measurement was done for two different sizes (0.1 mm and 0.2 mm). The linear (without the end stops) and non-linear frequency response functions for the small and large backslash sizes measured around the first natural frequency can be seen in Fig. 9b. The smaller gaps produce more significant non-linear behaviour than the larger gaps under the same excitation. It is assumed that other modes do not significantly influence the system behaviour around the first mode. Therefore, the first mode may be treated as a response of a SDOF system and the method proposed may be applied.

The measured FRFs were processed according to flow chart from Fig. 2. To illustrate the direct use of principal component scores, the PCS obtained from the FRFs are shown in Fig. B.1 together with the PCS of the training data. It can be seen that the FRFs measured without the non-linearity are very close to the

linear area of the graph although some overlap with the friction PCS can also be observed. On the other hand, the PCS of the FRFs that are affected by the gap lay clearly in the area of the clearance non-linearity.

Although the type of non-linearity can be estimated qualitatively from Fig. B.1, a more accurate and fully automatic qualitative decision can be made using the ANN. The same network was applied to these FRFs and the results of classification are summarized in Tab. 7. It is seen that non-linear behaviour

	no gap	small gap	large gap
low excitation	linear (70.4 %)/friction (29.1 %)	clearance (99.9 %)	clearance (99.9 %)
high excitation	linear (73.9 %)/friction (25.2 %)	clearance (99.9 %)	clearance (99.9 %)

Table 7: Characterization results for the cantilever beam

has been classified correctly with a high level of confidence. On the other hand, the analysis of the FRF measured without the end stops have revealed almost 30 per cent probability of friction in the structure. This, however, can be explained by the clamp in which micro-slip can cause this behaviour. Moreover, these results correspond to the observations made directly using principal component scores.

5.2. Under-platform damper with a complex contact interface

The experimental set-up seen in Fig. 10a allows evaluating the effect of an under-platform damper on the vibration behaviour of turbine blades. The design of the experimental rig and its relation to real turbine blades as well as details of the measurement process and numerical modelling are described in [21].

Some of the FRFs measured around the first mode of the structure in which the blades simultaneously vibrate in the first bending mode can be seen in Fig. 10b. As in the previous case, it is assumed that the first mode is not significantly influenced by the higher modes, and the method proposed may be applied. A stepped sine excitation with a decreasing frequency rate was used and the FRFs were measured using two non-contact laser Doppler vibrometers focused near the tip of each blade (see Fig. 10).

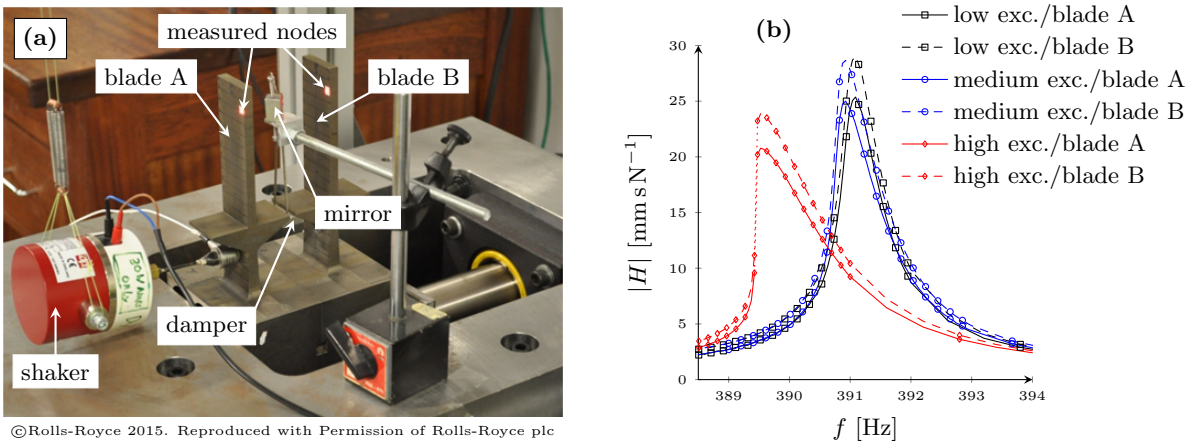

Figure 10: Under-platform damper: (a) experimental configuration (b) measured FRFs

Again, the measured FRFs were processed according to flow chart from Fig. 2 and the PCS are shown in Fig. B.2. It can be seen that no linear behaviour has been detected in the experimental test rig. Most of the measured PCS lay in the softening area although the PCS approach the linear and friction area under the low level of excitation.

To obtain the quantitative values, the same network was applied and the results are summarized in Tab. 8. In this case, no linear behaviour has been observed, not even on the lowest level of the excitation. The linear behaviour, however, was not expected even at low excitation levels since the damper is attached

	blade A	blade B
low excitation	softening (43.0 %)/friction (56.6 %)	softening (44.1 %)/friction (55.5 %)
medium excitation	softening (69.9 %)/friction (30.0 %)	softening (70.8 %)/friction (29.2 %)
high excitation	softening (99.6 %)	softening (99.7 %)

Table 8: Characterization results for the under-platform damper beam

and introduces the non-linear effects, albeit weak, into the structure. Under the low level of excitation the classification yielded almost equal probabilities of softening stiffness and friction, whereas classification of the FRFs measured under high excitation showed softening effect only. These results, although they do not directly relate to the under-platform damper's complex contact interface, reflect the effects observed in the FRFs. Under low excitation the amplitude is reduced with only a small frequency shift, whereas at high excitation levels the resonance frequency is strongly shifted and the jump in the response can be seen. The classification is consistent for the both blades although the FRFs that have been measured from blade A and B are slightly different.

6. Conclusion

A method for detection and characterization of non-linear behaviour from a single frequency response function has been presented in this paper. The method uses normalized single mode FRFs together with their Hilbert transform to derive a set of non-linearity indexes for an accurate and effective description of non-linear behaviour. Further reduction of these indexes via principal component analysis allows the creation of a compact neural network, which subsequently characterizes the non-linearities. The performance of the method was evaluated based on a number of test cases - some of which were numerical while others were experimental. It was found that the method is capable of detecting and characterizing non-linearities accurately while being robust in the presence of measured noise. Moreover, provided that a suitable neural network has been trained, the method works in a timely-fashion and avoids a subjective decision as this requires vast experience in the field. The successful characterization of two experimental cases, each with different types of non-linearity, demonstrates the robustness of the proposed method and its applicability to the experimentally measured FRFs. The method does not require any spatial model of the structure and therefore has great potential to become a fully automated tool for reliable characterization of well-separated non-linear modes.

Acknowledgements

The authors are grateful to Rolls-Royce plc for providing the financial support for this project and for giving permission to publish this work. This work is part of a Collaborative R&T Project "SAGE 3 WP4 Nonlinear Systems" supported by the CleanSky Joint Undertaking and carried out by Rolls-Royce plc and Imperial College. We would also like to thank Dr. Loïc Salles for providing the support when using FORSE and Mr. Luca Pesaresi for providing the measured data from the under-platform damper experimental rig.

References

[1] K. Worden, G. R. Tomlinson, Nonlinearity in structural dynamics: detection, identification and modelling, Institute of Physics Publishing, Bristol and Philadelphia, 2001.

[2] G. Kerschen, K. Worden, A. F. Vakakis, J.-C. Golinval, Past, present and future of nonlinear system identification in structural dynamics, Mechanical Systems and Signal Processing 20 (3) (2006) 505–592. doi:10.1016/j.ymssp.2005.04.008.

[3] D. E. Adams, R. J. Allemang, Survey of nonlinear detection and identification techniques for experimental vibrations, in: Proceeding of the International Seminal on Modal Analysis (ISMA), Leuven, 1998, pp. 269–281.

[4] K. Vanhoenacker, J. Schoukens, J. Swevers, D. Vaes, Summary and comparing overview of techniques for the detection of non-linear distortions, in: Proceeding of the International Seminal on Modal Analysis (ISMA), Leuven, 2012, pp. 1241–1256.
[5] K. A. Kragh, J. J. Thomsen, D. Tcherniak, Experimental detection and quantification of structural nonlinearity using homogeneity and Hilbert transform methods, in: Proceedings of the International Conference on Noise and Vibration Engineering, 2010, pp. 3173–3188.
[6] M. Aykan, H. N. Özgüven, Parametric identification of nonlinearity in structural systems using describing function inversion, Mechanical Systems and Signal Processing 40 (1) (2013) 356 – 376. doi:http://dx.doi.org/10.1016/j.ymssp.2013.03.016.
[7] S. M. Hosseini, T. A. Johansen, A. Fatehi, Comparison of Nonlinearity Measures based on Time Series Analysis for Nonlinearity Detection, Modeling, Identification and Control: A Norwegian Research Bulletin 32 (4) (2011) 123–140. doi:10.4173/mic.2011.4.1.
[8] M. Feldman, Hilbert transform in vibration analysis, Mechanical Systems and Signal Processing 25 (3) (2011) 735–802. doi:10.1016/j.ymssp.2010.07.018.
[9] A. d. Carri, D. J. Ewins, Topics in Modal Analysis, Volume 7: Proceedings of the 31st IMAC, A Conference on Structural Dynamics, 2013, Springer New York, New York, NY, 2014, Ch. A Systematic Approach to Modal Testing of Nonlinear Structures, pp. 273–286. doi:10.1007/978-1-4614-6585-0_25.
[10] A. Koyuncu, E. Cigeroglu, M. E. Yumer, H. N. Özgüven, Topics in Nonlinear Dynamics, Volume 1: Proceedings of the 31st IMAC, A Conference on Structural Dynamics, 2013, Springer New York, New York, NY, 2013, Ch. Localization and Identification of Structural Nonlinearities Using Neural Networks, pp. 103–112. doi:10.1007/978-1-4614-6570-6_9.
[11] R. Wardle, K. Worden, N. King, Classification of nonlinearites using neural networks, in: Proceeding of the International Modal Analysis Conference (IMAC), 1997, pp. 980–986.
[12] G. R. Tomlinson, Development in the use of the Hilbert transform for detectiong and quantifying non-linearity associated with frequency response functions, Mechanical Systems and Signal Processing 1 (2) (1987) 151–171. doi:10.1016/0888-3270(87)90068-9.
[13] M. Simon, G. R. Tomlinson, Use of the Hilbert transform in modal analysis of linear and non-linear structures, Sound And Vibration 96 (4) (1984) 421–436. doi:10.1016/0022-460X(84)90630-8.
[14] K. Worden, W. J. Staszewski, J. J. Hensman, Natural computing for mechanical systems research: A tutorial overview, Mechanical Systems and Signal Processing 25 (1) (2011) 4–111. doi:10.1016/j.ymssp.2010.07.013.
[15] A. Hot, G. Kerschen, E. Foltête, S. Cogan, Detection and quantification of non-linear structural behavior using principal component analysis, Mechanical Systems and Signal Processing 26 (1) (2012) 104–116. doi:10.1016/j.ymssp.2011.06.006.
[16] R. O. Duda, P. E. Hard, D. S. Stork, Pattern Classification, A Wiley-Interscience Publication, New York, 2001.
[17] M. Hagan, H. B. Demuth, M. H. Beale, Neural Network Design, MA: PWS Publishing, Boston, 1996.
[18] D. J. Ewins, Modal testing, theory, practice and application, Research studies press ltd., 2000.
[19] E. P. Petrov, D. J. Ewins, State-of-the-art dynamic analysis for non-linear gas turbine structures, Proceedings of the Institution of Mechanical Engineers, Part G: Journal of Aerospace Engineering 218 (3) (2004) 199–211. doi:10.1243/0954410041872906.
[20] L. Salles, L. Blanc, F. Thouverez, A. M. Gouskov, P. Jean, Dual Time Stepping Algorithms With the High Order Harmonic Balance Method for Contact Interfaces With Fretting-Wear, Journal of Engineering for Gas Turbines and Power 134 (3) (2012) 032503. doi:10.1115/1.4004236.
[21] L. Pesaresi, C. W. Schwingshackl, L. Salles, R. Elliott, A. Jones, J. Green, Numerical and experimental investigation of an under-platform damper test rig, in: Proceeding of the 11th International Conference on Engineering Vibration, Ljubljana, 2015, pp. 691–704.

Appendix A. Table of non-linearity indexes

NLI no.	Origin	Definition
1	[5]	$1 - \|R_{H\tilde{H}}(0)\|^2, \quad R_{H\tilde{H}}(\Delta\omega) = \int_{\omega_{\min}}^{\omega_{\max}} H(\omega)\tilde{H}(\omega+\Delta\omega)\mathrm{d}\omega$
2	[1, 12]	$\Re\left\{\frac{M_{\tilde{H}}^{(0)} - M_H^{(0)}}{M_H^{(0)}}\right\}, \quad M_H^{(0)} = \int_{\omega_{\min}}^{\omega_{\max}} H(\omega)\mathrm{d}\omega$
3		$\Im\left\{\frac{M_{\tilde{H}}^{(0)} - M_H^{(0)}}{M_H^{(0)}}\right\}$
4	[1, 12]	$\Re\left\{\frac{M_{\tilde{H}}^{(1)} - M_H^{(1)}}{M_H^{(1)}}\right\}, \quad M_H^{(1)} = \int_{\omega_{\min}}^{\omega_{\max}} \omega H(\omega)\mathrm{d}\omega$
5		$\Im\left\{\frac{M_{\tilde{H}}^{(1)} - M_H^{(1)}}{M_H^{(1)}}\right\}$
6	[1, 12]	$\Re\left\{\frac{M_{\tilde{H}}^{(2)} - M_H^{(2)}}{M_H^{(2)}}\right\}, \quad M_H^{(2)} = \int_{\omega_{\min}}^{\omega_{\max}} \omega^2 H(\omega)\mathrm{d}\omega$
7		$\Im\left\{\frac{M_{\tilde{H}}^{(2)} - M_H^{(2)}}{M_H^{(2)}}\right\}$
8	proposed	$\Re\left\{\frac{\tilde{\gamma_1} - \gamma_1}{\gamma_1}\right\}, \quad \gamma_1 = \frac{\int_{\omega_{\min}}^{\omega_{\max}} m(\omega)H(\omega)\mathrm{d}\omega}{\int_{\omega_{\min}}^{\omega_{\max}} m(\omega)\mathrm{d}\omega}$
9		$\Im\left\{\frac{\tilde{\gamma_1} - \gamma_1}{\gamma_1}\right\}$
10	proposed	$\frac{\tilde{\gamma_2} - \gamma_2}{\gamma_2}, \quad \gamma_2 = \int_{\omega_{\min}}^{\omega_{\max}} m(\omega)\left(\Re\{H(\omega)\}^2 + \Im\{H(\omega)\}^2\right)\mathrm{d}\omega$
11	proposed	$\frac{\tilde{\gamma_3} - \gamma_3}{\gamma_3}, \quad \gamma_3 = \int_{\omega_{\min}}^{\omega_{\max}} m(\omega)\left((\omega-\overline{\omega})^2 + \Re\{H(\omega)-\gamma_1\}^2 + \Im\{H(\omega)-\gamma_1\}^2\right)\mathrm{d}\omega$
12	proposed	$\Re\left\{\overline{G}\right\}, \quad \overline{G} = \frac{1}{\mathrm{n_{sl}}}\sum_{k=1}^{\mathrm{n_{sl}}} G(\omega_k), \quad G(\omega) = \tilde{H}(\omega) - H(\omega)$
13		$\Im\left\{\overline{G}\right\}$
14	proposed	$\sqrt{\frac{1}{\mathrm{n_{sl}}-1}\sum_{k=1}^{\mathrm{n_{sl}}}(G(\omega_k) - \overline{G})^2}$

Table A.1: Summary of non-linearity indexes

Appendix B. Principal component scores for experimental cases

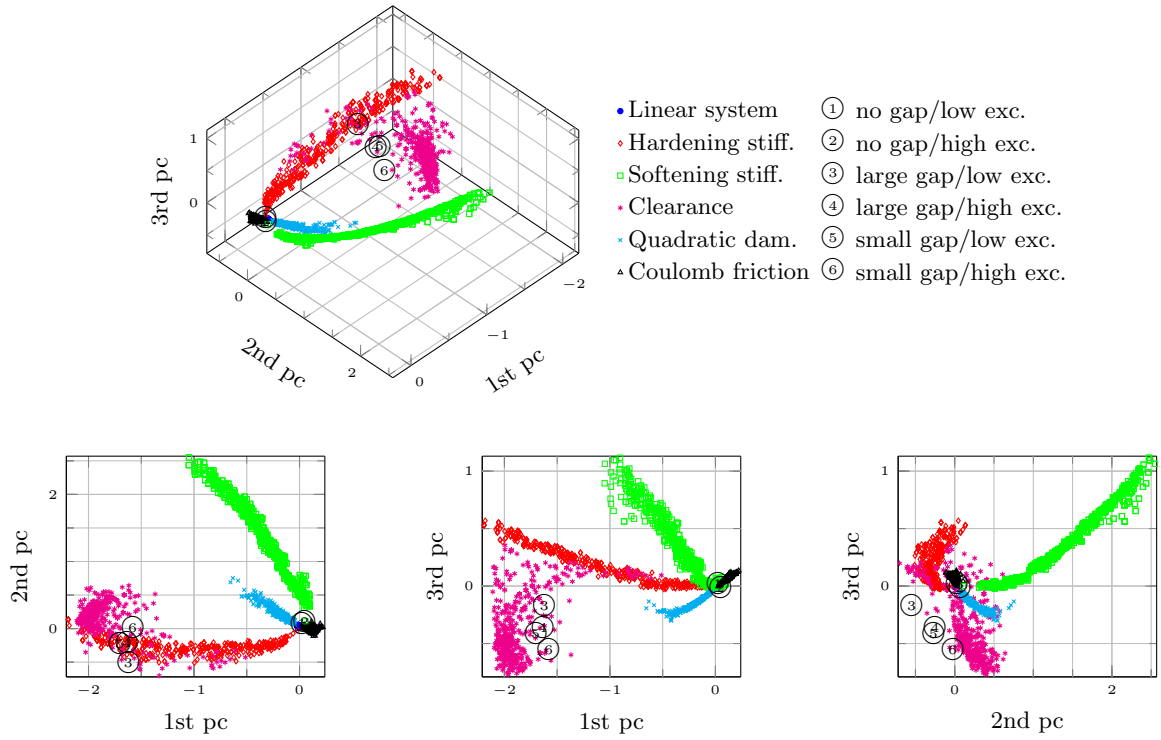

Figure B.1: Principal component scores of the cantilever beam: perspective view (top) and side views (bottom)

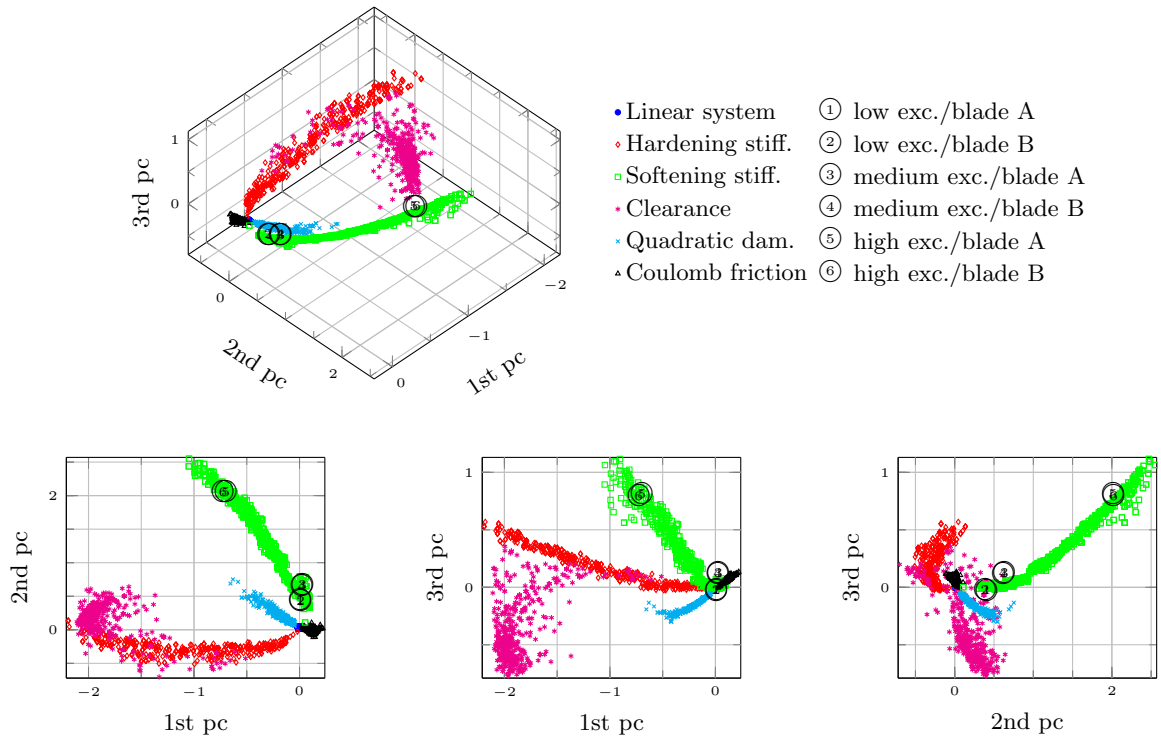

Figure B.2: Principal component scores of the under-platform damper: perspective view (top) and side views (bottom)